Time and Frequency Domain Characterization of Switching Losses in GaN FETs Power Converters

Marco A. Azpúrua, *Senior Member, IEEE*, Marc Pous, *Member, IEEE*, and Ferran Silva

***Abstract*—This paper presents a methodology for the time-frequency characterization of switching losses in Gallium Nitride Field Effect Transistors used in power electronics applications, particularly in DC-DC converters. Typically, switching losses are measured in the time-domain through the integration of the instantaneous power, that is, the product of the voltage multiplied by the current, during the turn-on and turn-off transients. Nonetheless, as novel power transistors allow for switching times in the nanosecond range, the accuracy of such measurements is compromised by the limitations of the probe-oscilloscope systems in terms of bandwidth and dynamic range. Here, we analyze the time-domain switching loss measurement method, and then, through a complementary setup we demonstrate how to validate the results in the frequency domain. A DC-DC half-bridge buck converter circuit based on the EPC2001C was used as a representative test sample. Less than 1% of difference in critical parameters such as rise-time, pulse width, state-levels and, switching frequency, is encountered between the time and frequency domain approaches. Moreover, the measurement uncertainty was analyzed and estimated to be between ±1% and ±8%. This work allows for highly confident switching loss measurements, a better understanding of the switching phenomena and of the measurement system performance.**

***Index Terms*— DC-DC power converters, measurement uncertainty, power transistors, switching loss, time-domain analysis.**

I. Introduction

NOWADAYS, Gallium Nitride (GaN) is a high-speed wide bandgap semiconductor widely employed in transistor manufacturing. GaN power transistors for power electronics applications have achieved better efficiency, faster response, and smaller size compared to silicon devices [1]. The switching speed of low voltage GaN switches can be two orders of magnitude higher than typical silicon MOSFETs [2]. Likewise, the on-state resistance/breakdown voltage tradeoff of GaN FETs has been reported to be three orders of magnitude better than Si-based power switching technology [3].

Power converters are one of the applications where there is widespread use of GaN devices. Generally, power converters comprise several switching devices and the main contributions to energy losses are related to them. In this regard, conduction loss depends on the on-state resistance (R_{on}), while the switching loss occurs at the turn-on and turn-off transients of the devices [4]. In comparison to Si MOSFET devices, GaN switches have lower capacitance and R_{on}, therefore, they allow more efficient power converters that can be driven at higher switching frequencies. In this regard, as switching frequencies increase in GaN power converters (> 1 MHz), the dynamic losses account for a larger portion of the total losses and their contribution to the converter power budget becomes dominant, typically more than 70% of the total losses.

To estimate the switching losses in GaN devices, theoretical models can be used with the information provided in the device datasheet as inputs. However, most theoretical models do not consider the influence of other circuit elements such as the driver, the converter topology, or the parasitic parameters affecting the switching process at high frequencies. Otherwise, SPICE simulations could be used to calculate switching losses, if a validated model for the switching device is available [4]. Nonetheless, such alternatives are not generally feasible for many GaN power converters. Typically, the datasheets of GaN switching devices do not specify switching losses, and validated SPICE models may not be widely accessible, even if remarkable progress has been made in that direction [5]–[7]. In consequence, measurements are required for characterizing the switching loss in many GaN devices working at high switching frequencies.

Switching loss is measured by integrating the product of the voltage across the switch and the current flowing through it over the duration of the switching transients. This is valid for both the turn-on and the turn-off transients. This time domain approach involves acquiring the voltage and current waveforms using an appropriate oscilloscope with a set of calibrated, compensated and de-skewed probes with suitable bandwidth and flat frequency response [8]. Even if, conceptually, the measurement method is straightforward, a number of challenges arise from the sharp switching transitions that can be reached by GaN devices [2], with rise/fall times in the nanosecond range and frequency components up to 1 GHz.

Consequently, to accurately measure switching losses in GaN power converters, the fidelity in the measured V/I waveforms is fundamental. Therefore, the probe-oscilloscope system has a major role to play in it [9]. Previous research investigated the complex influence of the probes-oscilloscope set in the current and voltage waveforms measured. In particular, in [10] the influence of the delay, distortion, and overshoot effects on the switching loss measurement error was

This research work is carried in the framework of the 16ENG06 ADVENT project. This project, 16ENG06 ADVENT, has received funding from the EMPIR programme co-financed by the Participating States and from the European Union's Horizon 2020 research and innovation programme. This work was supported by the Spanish "Ministerio de Ciencia e Innovación" under project PID2019-106120RB-C31 / AEI / 10.13039/501100011033.

M. A. Azpúrua, M. Pous, and F. Silva are with the Group of Electromagnetic Compatibility, Department of Electronic Engineering, Universitat Politècnica de Catalunya, 08034 Barcelona, Spain (e-mail: marco.azpurua@upc.edu; marc.pous@upc.edu; ferran.silva@upc.edu).

This article has been accepted for publication in a future issue of this journal, but has not been fully edited. Content may change prior to final publication. Citation information: DOI 10.1109/TPEL.2021.3112909, IEEE Transactions on Power Electronics

studied. Likewise, inverse probe models for correcting the previously mentioned sources of error have been proposed [11].

In a preceding conference paper from the authors, the analysis of the switching loss measurement method was presented and, from there, bandwidth, timing, and distortion correction considerations were defined for the probe-oscilloscope system. Subsequently, a top-down analysis was carried out for modeling and propagating the contributions to the switching losses' measurement uncertainty [12].

Here, we enhanced the prior analysis with a model and the time-frequency characterization of the switching losses in GaN FETs power converters. In this respect, we validate the switching loss measurements through characteristic parameters of the waveforms extracted from the spectrum measurements. The combination of time- and frequency-domain techniques, in conjunction with dynamic temperature assessments presented in [13] comprehends the multiphysics approach developed within the ADVENT project [14], which in this case has been applied to the characterization of the power losses GaN FET power converter applications combining hard switching and high switching frequencies.

II. Switching Losses Theoretical Model

To characterize the switching losses in high-speed GaN FETs for DC-DC power conversion applications it is important to begin with a model that allows understanding the parameters that must be measured in this regard [15].

Let us take as a reference the circuit of a half-bridge buck converter in Fig. 1. Here, the control switch (CS) and the synchronous rectifier (SR) are transistors, the high-side (Q1) and low-side (Q2) ones in Fig. 1, respectively. The state of the transistors is controlled through the gate-to-source voltage provided by the driver circuit. In the hard switching half-bridge converter presented below, the CS is recognized by a positive drain current (i_D) in the corresponding direction of the load current (I_L) flowing through the L_{out}. Commonly, half-bridge circuits are symmetric, which means Q1 and Q2 are identical.

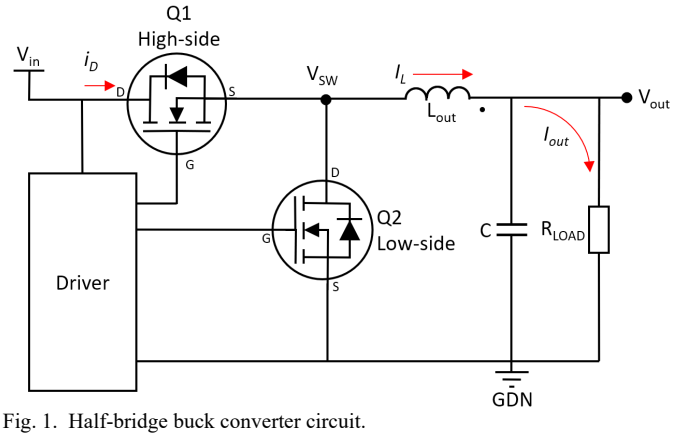

Fig. 1. Half-bridge buck converter circuit.

In the circuit in Fig. 1, the control switch is responsible for most of the dynamic losses in the circuit. Fig. 2 presents the simplified model for the waveforms during the turn-on and turn-off switching transitions in a half-bridge circuit with GaN transistors of low gate resistance. Here, during the turn-on transition, the gate-source voltage, V_{GS}, does not plateau because of the small input capacitance and Miller capacitance. After the initial current rise transition, V_{GS} continues rising, permitting the channel current to keep rising as well. The Miller capacitance contributes in reducing the slope of V_{GS} rise while the duration of the voltage turn-off transient is mostly determined by $Q_{(OSS,Q1)}+ Q_{(OSS,Q2}$, that is, the total charge on the switch node. The power losses during the turn-on transition can be split into two components: loss due to the output capacitance (C_{OSS}) and overlap losses caused by the simultaneous effect of the current and the voltage across the drain to source terminals. Regarding the turn-off transient, it is the opposite of a turn-on one. The key difference is that the I_L has the same polarity required to displace the output capacitance charges in both Q1 and Q2, charging up $C_{OSS,Q1}$ to the input voltage, and discharging $C_{OSS,Q2}$ to zero without incurring any ohmic power losses. Nevertheless, minor overlap losses occur during this transient time-frame, as the I_L continues to flow through the saturated channel until it arrives to the cutoff region. As with the turn-on transition, the actual turn-off overlap loss is a function of the speed of the gate driver.

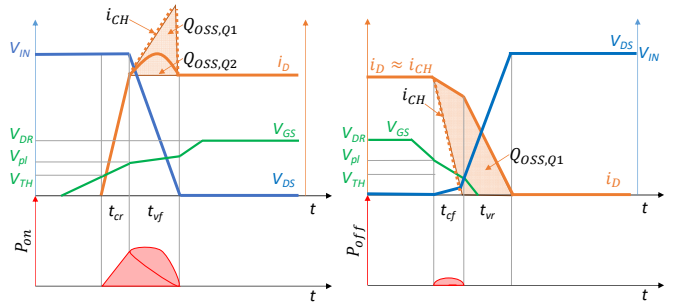

a) Turn-on transition b) Turn-off transition

Fig. 2. Simplified switching waveforms for a turn-on and turn-off transitions in a half-bridge circuit with GaN transistors of low gate resistance.

A. Turn-on losses

The turn-on losses are the combination of output capacitance (C_{OSS}) losses, P_{OSS}, and the overlap losses during the turn-on transition, $P_{on(overlap)}$, that is,

$$P_{on} = P_{OSS} + P_{on(overlap)}. \quad (1)$$

In symmetric half-bridge circuits, P_{OSS} can be estimated as,

$$P_{OSS} = f_{SW} Q_{OSS,V_{in}} V_{in} \quad (2)$$

where $Q_{OSS,V_{in}}$ is the charge of the output capacitance. C_{OSS} is a non-linear function of the drain-to-source voltage, therefore,

$$Q_{OSS,V_{in}} = \int_0^{V_{in}} C_{OSS}(v_{DS}) dv_{DS}\,. \quad (3)$$

Conversely, the turn-on overlap loss can be approximated as,

$$P_{ON(overlap)} = f_{sw} \int_{t_{ON}^-}^{t_{ON}^+} v_{DS}(t) i_D(t) dt \approx \frac{1}{2} V_{in} I_{L,ON} (t_{cr} + t_{vf}) f_{sw} \quad (4)$$

where $[t_{ON}^-; t_{ON}^+]$ is the turn-on transition interval, $I_{L,ON}$ is the inductor current during the turn-on transition, t_{cr} is the current rise time and t_{vf} is the voltage fall time.

In this regard, $I_{L,ON}$ is higher than I_{out} due to the current ripple, I_{ripple}

$$I_{L,ON} = I_{out} - \frac{I_{ripple}}{2} = I_{out} - \frac{V_{in} - V_{out}}{2 f_{sw} L_{out}} D \quad (5)$$

Concerning the current rise time, it is determined by the charge required to transition i_D, which requires that the gate-charge transition between the threshold voltage, V_{TH}, and the plateau voltage, V_{pl}, that is Q_{GS2}. The dynamic gate current, I_G, is given by the ratio between the driver on-voltage, $V_{driver(on)}$, and the gate-to-source voltage, V_{GS}, and the gate resistance for the turn-on path, $R_{g(on)}$. Accordingly,

$$t_{cr} = \frac{Q_{GS2}}{\frac{V_{driver(on)} - V_{GS}}{R_{g(on)}}} = \frac{Q_{GS2}(R_g + R_{pu} + R_{CSI})}{V_{driver(on)} - \left(\frac{V_{TH} + V_{pl}}{2}\right)} \quad (6)$$

where R_g is the gate resistance (internal and external), R_{pu} is the driver pull-up resistance and R_{CSI} is the equivalent common-source inductance resistance.

On the other hand, the voltage fall time is given by,

$$t_{vf} \approx \left(\frac{Q_{OSS,Q1} + Q_{OSS,Q2}}{V_{driver(on)} - V_{pl}}\right)\left(\frac{1}{g_{fs}} + \frac{2(R_g + R_{pu})C_{RSS,Q1(0\,V)}}{C_{OSS,Q1(0\,V)} + C_{OSS,Q2(V_{in})}}\right) \quad (7)$$

where $Q_{OSS,Q1} + Q_{OSS,Q2}$ is the total displacement charge, g_{fs} is the transconductance of the transistor Q1 and C_{RSS} is the non-linear reverse transfer capacitance.

B. Turn-off losses

As shown in Fig. 2-b), low gate resistance GaN switches have low turn-off losses because channel current has already depleted before the drain-to-source voltage. This is caused by the gate voltage falling below the threshold before dv_{ds}/dt becomes high, avoiding the Miller plateau entirely. Referring to an analysis similar to the previous one, the current fall time can be calculated according to

$$t_{cf} = \frac{Q_{GS2}}{\frac{V_{pl} + V_{TH}}{2} - V_{driver(off)}} = \frac{Q_{GS2}(R_g + R_{pd})}{\frac{V_{pl} + V_{TH}}{2} - V_{driver(off)}} \quad (8)$$

where $V_{driver(off)}$ is the driver off voltage (typically 0 V) and $R_{g(off)}$ is the gate resistance during the off transition and R_{pd} is the driver pull-down resistance. According to the analysis made in [15], after several approximations, the turn off losses can be estimated as,

$$P_{OFF(overlap)} = \frac{\frac{1}{12}\left(I_{L,OFF} t_{cf}\right)^2}{C_{OSS,Q1(0\,V)} + C_{OSS,Q2(V_{in})}} \quad (9)$$

Throughout the model presented in this section, it is, in principle, possible to estimate the switching losses in GaN FETs. However, the model is mostly applicable when the non-linear output capacitance is known. From the standpoint of the designer that is interested in determining the losses a certain GaN FET will experience in the intended application, this would be only possible if the operating conditions matched those specified in the datasheet.

However, the situation above is not general enough to cover most cases and switching loss measurements are usually required. In this regard, it is fundamental not to forget that with a rise time in the nanosecond range, that is, with significant spectral components up to approximately 1 GHz, measuring switching losses requires appropriate measurement equipment, measurement techniques and requires attention to test methodologies, as will be explained in the next section.

C. Switching loss prediction model operation flow

To evaluate the switching losses according to the model described previously, we must start from the static and dynamic characteristics of the GaN power transistor. Usually, such parameters are defined in the component datasheet for a given operating range and test conditions. Likewise, model variables related to the driver circuit and factors from other elements in the power converter circuit can be taken from their respective specifications as well.

The flowchart in Fig. 3 illustrates the operational flow of the proposed model. A color code is used to represent how the inputs of the model propagate to the desired outputs through intermediate calculations. In each step, the corresponding equations were previously presented.

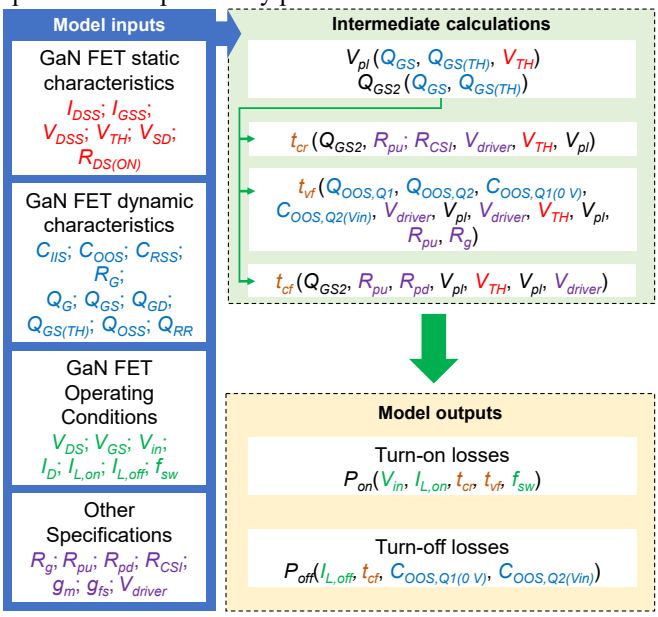

Fig. 3. Switching loss model operational flowchart.

If the device is used outside its specified range, the model above might not be valid. Therefore, any relevant comparison between the measured and predicted switching losses must be made at operating conditions where the static and dynamic characteristics of the GaN FET are accurately known.

III. Switching Losses Measurement Method

The instantaneous value of the power losses, $p(t)$, in a switching device is given by the product of the drain-source voltage, $v_{DS}(t)$, and the drain current $i_D(t)$. In that sense, the total switching energy loss, E_{SW}, is given by,

$$E_{SW} = E_{on} + E_{off} = \int_{t_{ON}^-}^{t_{ON}^+} p(t)dt + \int_{t_{OFF}^-}^{t_{OFF}^+} p(t)dt \quad (10)$$

where $[t_{ON}^+, t_{ON}^-]$ and $[t_{OFF}^+, t_{OFF}^-]$ are the time intervals of the turn-on and turn-off transitions, respectively. It is vital to realize that the switching time interval ends when the waveform oscillations have been completely damped [16].

Consequently, the measurement of losses in switching devices requires synchronous measurement of $v_{DS}(t)$ and $i_D(t)$.

This article has been accepted for publication in a future issue of this journal, but has not been fully edited. Content may change prior to final publication. Citation information: DOI 10.1109/TPEL.2021.3112909, IEEE Transactions on Power Electronics

In principle, this is performed with an oscilloscope where the voltage waveform is sensed directly by using passive and/or differential probes while the current waveforms are measured through resistive shunts.

However, the measurement of the switching waveforms is sensitive to offset, timing (skew), and distortion errors. Therefore, voltage and current waveform measurements must be performed considering the following best practices.

A. General considerations

Firstly, a suitable measurement setup must be used to accurately measure high-speed switching waveforms. For instance, for measuring switching voltage waveforms, the combined rise time of the oscilloscope, t_s, and of the passive/differential probe, t_p, must be small in comparison to the actual 10 % - 90 % edge time, t_e, of the voltage waveform to be measured [2]. This means,

$$t_{meas} = \sqrt{t_s^2 + t_p^2 + t_e^2} \leq (1 + \Delta) t_e \,, \tag{11}$$

where Δ is the maximum timing error allowable according to the required measurement timing accuracy. Consequently, the combined (3 dB) bandwidth of the oscilloscope-probe system shall satisfy the condition in (11), that is,

$$BW_{3\,dB} \geq \frac{0.35}{\sqrt{t_s^2 + t_p^2}} = \frac{0.35}{\left(\sqrt{2 + \Delta}\sqrt{\Delta}\right) t_e} \,. \tag{12}$$

On the other hand, measuring the current waveform is challenging because oscilloscope current probes based on Hall effect and Rogowski sensors have shortcomings for this application in terms of their bandwidth. Alternatively, Hall [17] and Rogowski [18] broadband sensors for in-circuit current measurement are still limited to a few megahertz (DC – 10 MHz). On the other hand, RF current probes are generally large for fitting in the power converter, and even when it is possible to do it, the insertion impedance of the current probe is significant compared to the circuit, thus adding uncertainty to the measurement. Therefore, in practice, the current sensing technologies mentioned above are not suitable for this purpose. Contrariwise, high bandwidth current sensing resistors (1 GHz) such as coaxial shunts are the most recommended alternative for transforming the switching current waveform into a voltage signal to be measured [2].

In addition to the previous considerations, a set of best practices must be followed to ensure accurate switching loss measurements. The most important ones are correcting offset errors, employing de-skew procedures, enhancing the dynamic range and reducing the waveform noise by adequately configuring the oscilloscope acquisition mode and using the appropriate probe tip and grounding to minimize the ground loop inductance [8], [12], [19]

The above-mentioned recommendations are necessary, but not sufficient, to ensure an accurate measurement of the switching losses. This is because the probe-oscilloscope system produces distortion in the waveform, particularly when the probe's input capacitance is of the same order of magnitude as the capacitance of the device under test [20]. The next subsection analyzes the distortion of the probe-oscilloscope system through circuit modeling and simulation.

B. Waveform distortion correction

As the bandwidth of the switching waveforms increases, the parasitic effects that limit the response of the probe-oscilloscope system emerge and the waveform distortion produced by them can significantly alter the measurements.

In line with the above, let $x(t)$ be an input signal, and $y(t)$ be the corresponding measured (output) waveform; then,

$$y(t) = p(t) * x(t) + n(t) \tag{13}$$

where $p(t)$ is the probe-oscilloscope system impulse response and $n(t)$ is the noise in the measurements. However, if the probe-oscilloscope system is assumed to be linear time-invariant (LTI) and that the noise is negligible, then the complex value transfer function of the probe-oscilloscope system can be expressed as the frequency response, $P(j\omega)$,

$$P(j\omega) = |P(j\omega)| \angle \varphi(j\omega) = \frac{Y(j\omega)}{X(j\omega)} \tag{14}$$

where $X(j\omega)$ and $Y(j\omega)$ are the Fourier transforms of system input and output, respectively.

Therefore, if the probe-oscilloscope system frequency response is known and if the Fourier transform exists for $x(t)$ and $y(t)$, the amplitude and phase distortion caused by the measurement process can be corrected.

Now, let $y(t)$ to be periodic with period T, that is, $y(t)=y(t+T)$. In consequence, $y(t)$ can be written a Fourier series,

$$y(t) = c_0 + \sum_{n=1}^{\infty} |c_n| \cos(n\omega_0 t + \theta_n) \tag{15}$$

where $\omega_0 = 2\pi/T$. The constant coefficient in (15), c_0, is the average amplitude of the waveform over one period [21], that is

$$c_0 = \frac{1}{T} \int_0^T y(t) dt \tag{16}$$

whereas magnitude and phase of the harmonic components of the Fourier series are given by

$$c_n = |c_n| e^{j\theta_n} = \frac{2}{T} \int_0^T y(t) e^{-jn\omega_0 t} dt \,. \tag{17}$$

Consequently, in steady-state, $x(t)$ can be rewritten as the superposition of sinewaves in (18),

$$x(t) = \frac{c_0}{P_0} + \sum_{n=1}^{\infty} \frac{|c_n|}{P_n} cos(\omega_n t + \theta_n - \varphi_n) \tag{18}$$

where $\omega_n = n\omega_0$ is the angular frequency of the n-th harmonic component and $P_n \angle \varphi_n$ is the phasor obtained by evaluating $P(j\omega)$ at ω_n for n=1,2,3…

In practice, the number of harmonic components in (8) can be limited according to the measurement system bandwidth in order to avoid the non-realizable infinite summation. Thus, if B is the bandwidth of the measurement system then the order of the highest frequency harmonic, N, would be given by,

$$N = BT \,. \tag{19}$$

The transfer function required to perform the distortion correction of the probe-oscilloscope system can be extracted

This article has been accepted for publication in a future issue of this journal, but has not been fully edited. Content may change prior to final publication. Citation information: DOI 10.1109/TPEL.2021.3112909, IEEE Transactions on Power Electronics

from circuit models. Circuit models are particularly helpful because they are easy to simulate and help to understand the effect of the parasitic elements in the frequency response of the measurement system. For providing realistic correction factors, the probe-oscilloscope system models must be fitted and validated using calibration data and the instrument specifications.

In what follows, passive voltage probes are used for measuring voltage waveforms while coaxial current shunts are used for measuring current waveforms. In what follows both types of transducers will be analyzed.

C. *The frequency response of passive voltage probes*

Fig. 4 shows a probe-oscilloscope circuit model for a generic passive voltage probe. In this model, the tip, the cable, the compensation circuit, and the oscilloscope impedance are considered since they influence the measured voltage.

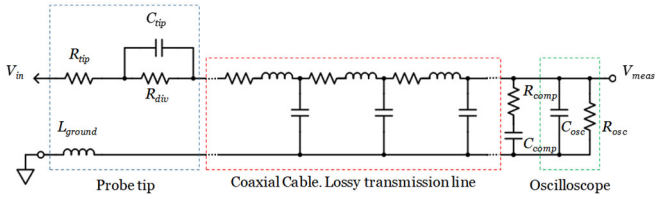

Fig. 4. Probe-oscilloscope model for a generic passive voltage probe.

As a particular example, let us tune the lumped and distributed parameters (resistances, capacitances, and inductances) in the model above according to the specified frequency response of the measurement system formed by the passive voltage probe TPP1000 from Tektronix and the Digital Real-Time sampling Oscilloscope (DRTO) DPO5104B from the same manufacturer [22], [23]. Here, R_{osc} is assumed to be 1 MΩ as stated in the oscilloscope specifications for high impedance measurements and R_{div} will depend on the attenuation factor, which means that for a DC voltage division factor of 10, R_{div} must be 9 MΩ. It is also specified that both elements have a 3 dB-bandwidth of 1 GHz. Accordingly, the theoretical rise time (10%-90%) of the oscilloscope is 350 ps at full bandwidth. In such conditions, the oscilloscope input impedance is set to 50 Ω and C_{osc} is given by,

$$C_{osc} = \frac{t_{10\%-90\%}}{Z_{osc} \times \ln\left(\frac{90\%}{10\%}\right)} \approx 3.1 \text{ pF} \qquad (20)$$

Moreover, in [19] it is reported that L_{loop} is 10 nH if the ½'' ground spring is used. From the TPP1000 specifications, it is known that its cable is 1.3 m ± 3 cm long. Finally, the typical probe's input impedance is provided in [22].

Therefore, the values for the lumped and distributed elements shown in Fig. 4 have been selected and tuned for satisfying the before mentioned conditions.

After performing an AC sweep analysis with NI Multisim 14.2, the results of the input impedance of the model are in excellent agreement with the TPP1000 specifications. Consequently, the probe simulation model was considered valid and it is reliable for estimating the probe transfer function through simulation.

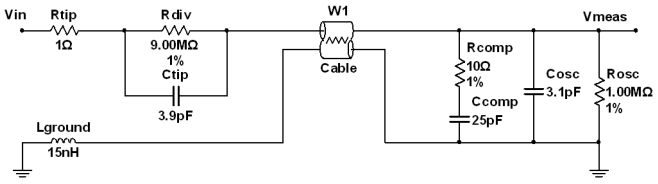

Fig. 5. Circuit model for the passive voltage probe TPP1000 from Tektronix.

Hence, the simulated frequency response of the TPP1000-DPO5104B probe-oscilloscope system is shown in Fig. 5. It is verified that the proposed model 3 dB cutoff frequency is approximately 1 GHz. Likewise, the flat frequency response exhibited by the probe in both magnitude and phase up to 100 MHz indicates that the probe-oscilloscope distortion might be neglected without significantly compromising the measurement's accuracy for waveforms with spectral content limited to 100 MHz. Conversely, it is evident that amplitude and phase distortion correction is mandatory when measuring high-speed switching waveforms.

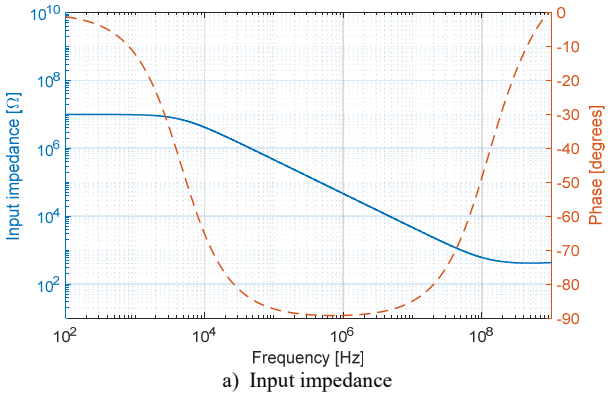

a) Input impedance

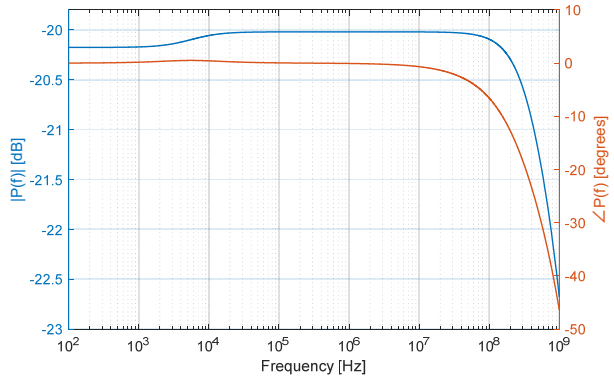

b) Transfer function

Fig. 6. The response of the validated circuit model of the TPP1000-DPO5104B probe-oscilloscope system.

D. *The frequency response of coaxial current shunts*

A shunt is a resistor across which a voltage is measured for sensing the current flowing through it. Hence, the shunt resistance in direct current (DC) conditions, R_{shunt}, is usually specified as the voltage-current conversion factor. For power electronics applications suitable R_{shunt} values are, typically, in the range of milliohms. In general, keeping R_{shunt} low allows reducing the impact of the shunt voltage drop in the circuits and minimizes the power dissipated in the shunt, thus reducing thermally induced resistance drift.

This article has been accepted for publication in a future issue of this journal, but has not been fully edited. Content may change prior to final publication. Citation information: DOI 10.1109/TPEL.2021.3112909, IEEE Transactions on Power Electronics

On the other hand, for alternating current and high-speed current waveform measurements (broadband frequency content), it is necessary to characterize the frequency response of the shunt impedance, Z_{shunt} (f). Shunts have an intrinsic inductance, which is influenced by their design structure [24]. The shunt inductance, L_{shunt}, is the key parameter limiting its frequency response. Considering a simple series RL circuit mode, $Z_{shunt}(j\omega) = R_{shunt} + j\omega L_{shunt}$, the shunt's 3 dB cutoff frequency, f_c, is the frequency at which R_{shunt} is equal to the shunt's reactance,

$$f_c = \frac{R_{shunt}}{2\pi L_{shunt}} . \quad (21)$$

Bearing in mind we require measuring the switching waveforms of GaN devices, f_c must be at least equal to the bandwidth of the rest of the measurement system. This requires the shunt inductance to be in the femtohenry range, that is, almost nulling the magnetic flux enclosed by the measuring loop.

In that sense, coaxial shunts, formed by two coaxial tubes that carry current in opposite directions, cancel the magnetic field inside the inner hollow tube. This inner tube is made of resistive material and when the leads are attached to the inner surface no flux linkage limits the shunt response. However, in this case, the shunt time response is determined by the propagation velocity of the signal through the shunt foil and the thickness of the sheet metal of the inner tube. The delay in response due to skin effect increases with tube thickness and conductivity. It follows that, for a fast response, a thin tube of highly resistive material is required. [25].

Therefore, the impedance characteristic of the coaxial current shunt is primarily flat from DC to the cutoff frequency (21). Hence, the equivalent L_{shunt} of the series RL circuit model can be calculated from its rise time. Experimentally, the shunt rise time (10%-90%) can be calibrated using a step function of current produced by a coaxial line pulse generator. In consequence,

$$L_{shunt} = \frac{R_{shunt} \cdot t_{10\%-90\%}}{\ln\left(\frac{90\%}{10\%}\right)} . \quad (22)$$

As an example, let us examine the coaxial shunt SDN-414-05 from T&M Research Products, Inc. Its nominal resistance is 50 mΩ and its specified rise time is 0.18 ns. The rise time has been calibrated using a reference pulse with di/dt > 10^{12} A/s. According to (22), this means $L_{shunt} \approx 4{,}1$ fH and $f_c \approx 2$ GHz. To the best of authors' knowledge, nowadays, only SDN-414 series from T&M Research Products, Inc. offers a suitable performance for GaN switching waveform measurements.

IV. Validation of the Switching Losses using Frequency-Domain Methods

The main concern when analyzing the high-speed switching waveforms is that the oscilloscope-probe system response time is comparable to, or even higher than, the rise and fall time of the measured signal, thus compromising the accuracy of the switching loss measurements. Nowadays, even high-bandwidth real-time oscilloscopes and their probes have a combined rise time that might be comparable to the switching times that characterize GaN FETs. Therefore, it is important to determine if the probe-oscilloscope system bandwidth is enough to measure the switching waveforms without significant distortion due to its band-limiting effect, that is, a distortion that cannot be corrected through the methods explained in the previous section.

For that purpose, the measurement of the frequency spectrum of the switching waveforms can be used to determine the signal bandwidth, and therefore, of its rise/fall time. According to the model in Section II, the switching waveforms are periodic and can be represented to a succession of trapezoid pulses. Therefore, its spectrum is calculable as a Fourier series (15). In this regard, it can be demonstrated that the n-th harmonic components of the trapezoid pulse is,

$$|c_n| = 2A\frac{\tau}{T}\left(\frac{\sin(\pi n f_{SW} t_r)}{\pi n f_{SW} t_r}\right)\left(\frac{\sin(\pi n f_{SW}\tau)}{\pi n f_{SW}\tau}\right) \quad (23)$$

$$\theta_n = -\pi n(\tau + t_r) f_{SW} \quad (24)$$

where A is the pulse amplitude, τ is the pulse width, T is the pulse period, f_{SW} is the switching frequency, t_r is the rise time.

If the amplitude of the harmonic components is plotted versus frequency in a log-log scale, as shown in Fig. 7, it is possible to identify that the envelope of the spectrum can be described by three regions where the slope of the envelope is approximately constant [21]. By finding the knee frequencies (f_{knee}), that is, the frequencies at which the slope of the spectrum envelope changes, it is possible to estimate indirectly the most relevant timing parameters of the waveform, such as the pulse duration and the rise time [26]. Knee frequencies can be accurately estimated by least square fitting the amplitude spectrum envelope to the piece-wise linear model represented in Fig. 7.

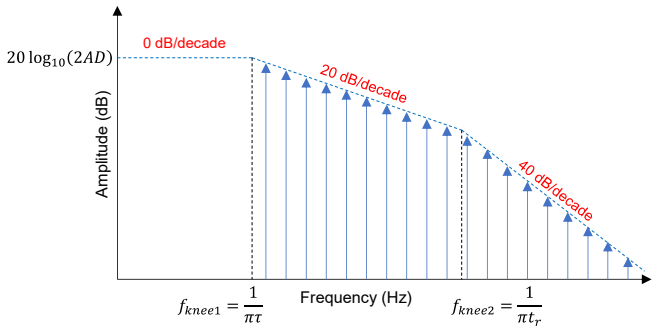

Fig. 7. Envelope of the switching waveform spectrum.

Likewise, from the switching waveform spectrum it is also possible to measure the pulse amplitude, the switching frequency, and the duty cycle, D. In this regard, it is important to notice the effect of the duty cycle in the spectrum bounds shown in Fig. 7. For instance, when D=50% only odd harmonics are present, otherwise the spectrum contains even harmonics as well. In terms of the envelope of the spectrum, the influence of D in the spectral bounds is related to the amplitude of the DC level and to the value of the first knee frequency, which is inversely proportional to D.

This article has been accepted for publication in a future issue of this journal, but has not been fully edited. Content may change prior to final publication. Citation information: DOI 10.1109/TPEL.2021.3112909, IEEE Transactions on Power Electronics

Therefore, in this manner, frequency-domain methods can be used to validate the time-domain parameters involved in the switching loss measurement.

V. Methodology

The device under test (DUT) is the EPC2001C enhanced mode GaN FET from Efficient Power Conversion Corporation. The DUT is driven in a half-bridge buck converter circuit implemented in the evaluation board LMG1205HBEVM from Texas Instruments, as shown in Fig. 8.

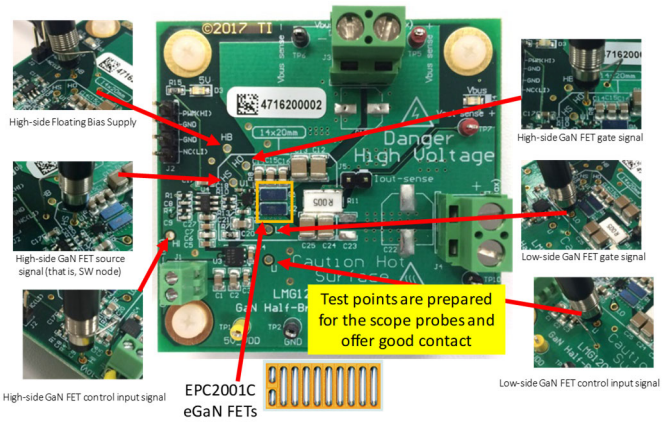

Fig. 8. Evaluation board "LMG1205HBEVM" using the EPC2001C eGaN FET.

The switching losses were characterized at three different switching frequencies, 100 kHz, 1 MHz, and 5 MHz, corresponding to the minimum, optimum and maximum values for the specified switching frequency range. Likewise, the load was controlled, and the output current was set 0, 1 A and 5 A using an Electronic Load BK 8500. The input voltage and the duty cycle were fixed at 20 V and 50%, respectively. The PWM signal was generated using a pulse function arbitrary generator model 81150a from Keysight.

The current and voltage waveforms measurements were performed using an oscilloscope Tektronix DPO5104B and using either passive probes TPP1000, differential probes TDP1500. The current was sensed using the SDN-414-05 from T&M Research Products, Inc. The probe-oscilloscope combined time is lower than 500 ps. The high side current and voltage waveforms were measured simultaneously, using two de-skewed, offset corrected and, DC coupled oscilloscope channels. A sampling frequency of 5 GSa/s was employed, and the bandwidth was set to 1 GHz. The jitter in the signals was measured and considered negligible (in all the cases, approximately 1 ps). Therefore, the average acquisition mode (averaging factor of 20x) was employed for reducing the noise without adding significant waveform distortion. The voltage drop in the shunt resistor (up to 25 mV) had a minor influence on the measurements. The ground spring of the passive probe was soldered to the test point ground for improving repetitiveness and for reducing the ground connection inductance.

Final measurements were performed inside an anechoic chamber as shown in Fig. 9 to avoid coupling ambient sources of RF noise. This consideration is important to improve the signal to noise ratio in the measurements. The RF noise coupled into the measurements cannot be filtered because the waveforms have a bandwidth in the order of hundreds of megahertz. Filtering would smooth the edges of the waveforms, thus causing errors in the magnitude of switching losses.

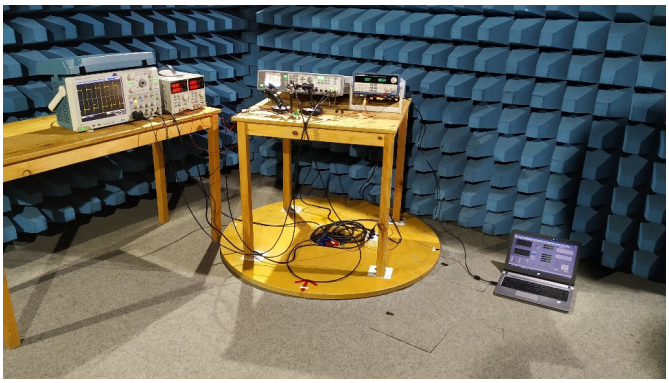

Fig. 9. Measurement setup for characterisation of the power losses of the EPC2001C.

VI. Results

A. Switching node waveform parameters

The rise time (10% - 90%), the fall time (90% - 10%), duty cycle, the deviation from the switching frequency (Δf_{sw}), state levels, and total jitter were measured for each operating condition. The measured switching node waveform parameters are in Table I.

The voltage waveforms in the switching node were acquired with a record length equal to 10 periods of the nominal switching frequency. The estimates of t_r, t_f, D, and Δf_{sw} were calculated for each period and are reported in the following table as their mean value. The jitter was calculated as the standard deviation of the pulse period. State levels were calculated using the histogram method [27].

TABLE I
SUMMARY WAVEFORM PARAMETERS FOR THE SWITCHING NODE WAVEFORM

Waveform parameters (Settings: V_{in} = 20 V; D = 50%; Temp = 25 ºC ± 1,5 ºC)								
f_{sw} (MHz)	I_L (A)	t_r (ns)	t_f (ns)	D (%)	Δf_{sw} (Hz)	Jitter (ps)	Off-state (V)	On-state (V)
0.1	0	5.50	5.52	49.97	0.195	1.82	1.004	19.549
0.1	1	7.00	4.94	49.96	0.187	9.06	0.979	19.508
0.1	5	1.87	3.63	49.90	0.192	1.28	0.716	19.758
1	0	2.74	1.97	49.71	1.912	0.40	0.777	19.106
1	1	1.62	6.43	49.64	1.737	0.39	0.950	19.162
1	5	1.53	4.54	49.55	1.899	0.22	0.886	19.026
5	0	3.03	1.93	47.74	1.160	1.15	0.873	19.063
5	1	3.16	10.38	47.47	10.881	1.189	0.821	18.885
5	5	2.10	4.97	42.85	8.238	0.8036	0.718	18.712

B. Switching loss measurements

On the left-hand side of the plots in Fig. 10, the corrected drain-source voltage and drain current measured in the control switch transistor (Q1) for the turn-on transition are shown. Conversely, in the right-hand side plots of Fig. 10, the instantaneous power is displayed in the red trace, while the turn-on energy loss corresponds to the area shadowed in light-red.

This article has been accepted for publication in a future issue of this journal, but has not been fully edited. Content may change prior to final publication. Citation information: DOI 10.1109/TPEL.2021.3112909, IEEE Transactions on Power Electronics

From the results, it is observed that the shape of the edges in the waveforms is sensitive to the changes in load conditions and switching frequency. For that reason, it is of key importance to characterize the device dynamically and in realistic operating conditions. This observation might be related to non-linear effects in the GaN FET, however, their influence is not investigated in this work.

The measured switching energy losses are compared with its estimated value calculated with the model presented in Section II and using the technical specifications in the EPC2001C datasheet [28]. The experiment results are in excellent agreement (less than 5% of difference) with respect to the theoretical value of the switching losses, as it is shown in Table II.

TABLE II
SWITCHING LOSSES FOR THE EPC2001C AT THE SPECIFIED OPERATING CONDITIONS

f_{sw} (MHz)	I_L (A)	Temp (ºC)	$E_{on(measurements)}$ (µJ)	$E_{on(model)}$ (µJ)	Difference (%)
0.1	1	25	0.249	0.239	4.50%
1	1	25	0.203	0.202	0.79%
5	1	25	1.700	1.694	0.38%
0.1	5	25	0.695	0.688	0.29%
5	5	25	0.849	0.884	-4.14%

C. *Frequency domain validation*

For evaluating in the frequency domain the parameters of the switching waveforms, a set of near filed probes HZ530 from HAMEG (Rohde & Schwarz) and a spectrum analyzer FSL18 from Rohde & Schwarz (9 kHz – 18 GHz) were used. The near field probe kit comprises three types of probes, one for the electric field, one for magnetic field and one for high-impedance voltage measurements. The frequency response of the field probes was known from their specifications and calibration reports in the 100 kHz – 1 GHz frequency range.

For measuring the spectrum of the voltage waveform, the high-impedance probe was employed. It has an input capacitance of 2 pF, which is half of the input capacitance provided by the high-impedance passive prove TPP1000 from Tektronix used for the time-domain measurements. During frequency domain measurements, the oscilloscope probes were disconnected.

Although a complete analysis of the measurement uncertainty for frequency domain measurements is not developed, a coarse uncertainty estimation is delivered. The high impedance probe factor is known with a tolerance of ±0.5 dB and the level measurement uncertainty of the spectrum analyzer is ±0.5 dB for signals below 3 GHz. After combining both contributions, the estimated measurement uncertainty for the spectrum amplitude is ±8.5%.

Fig. 11 shows a comparison of the spectrum of the switching node voltage measured in the frequency domain and the corresponding one calculated from time-domain measurement at operating at V_{in}=20 V, D=50%, and I_L=1 A and for the switching frequencies 100 kHz, 1 MHz, and 5 MHz. In all cases, there was observed a good agreement between the envelope of the spectrum of the voltage signal either if measured directly in the frequency domain or if calculated from the time domain waveforms.

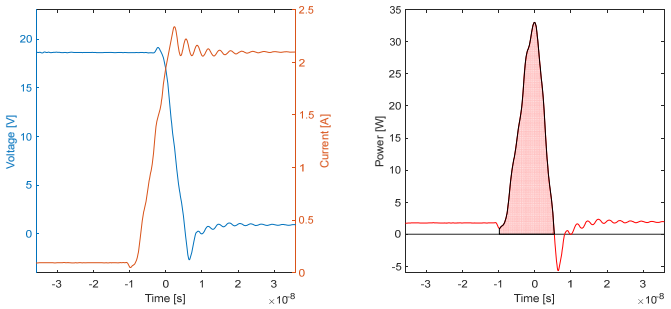

a) f_{sw} = 100 kHz and I_L = 1 A.

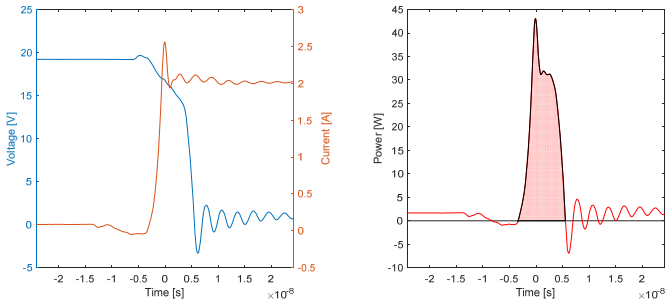

b) f_{sw} = 1 MHz and I_L = 1 A.

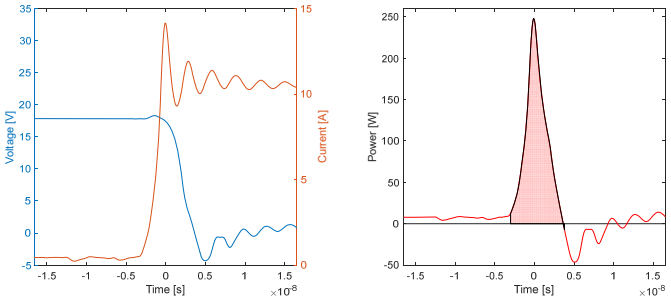

c) f_{sw} = 100 kHz and I_L = 5 A.

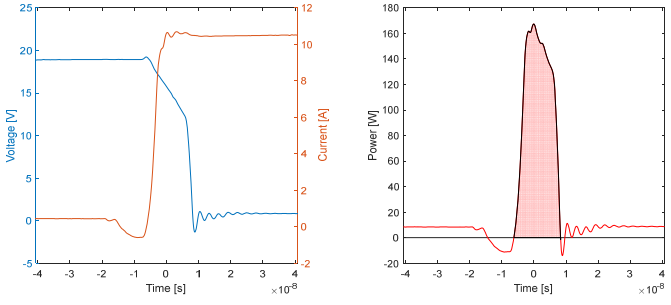

d) f_{sw} = 1 MHz and I_L = 5 A.

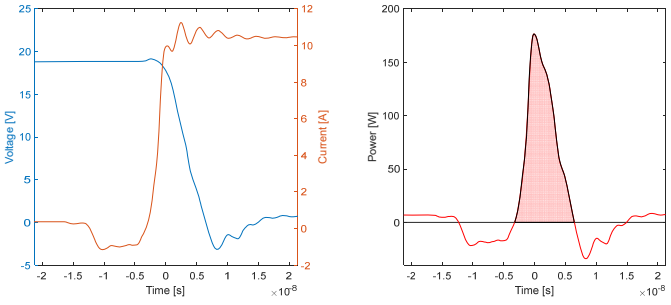

e) f_{sw} = 5 MHz and I_L = 5 A.

Fig. 10. Switching loss for the turn-on transition for different test conditions.

This article has been accepted for publication in a future issue of this journal, but has not been fully edited. Content may change prior to final publication. Citation information: DOI 10.1109/TPEL.2021.3112909, IEEE Transactions on Power Electronics

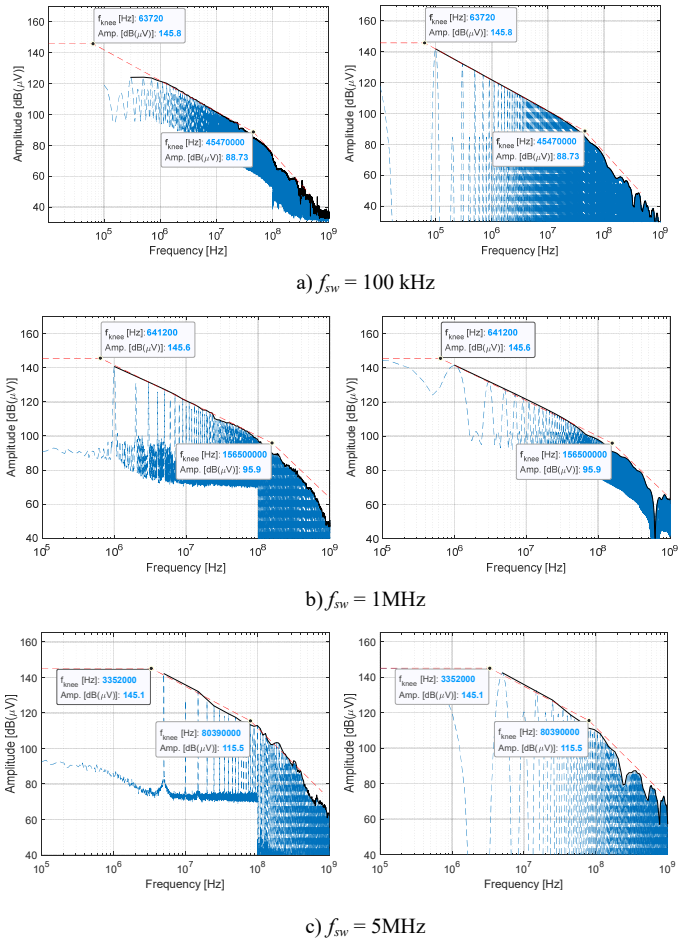

a) f_{sw} = 100 kHz

b) f_{sw} = 1MHz

c) f_{sw} = 5MHz

Fig. 11. Spectrum of the switching node voltage waveform for the DUT operating at V_{in}=20 V, D=50%, I_L=1 A and temperature = 25 ºC ± 1,5 ºC. Subfigures to the left correspond to the direct measurements of the spectrum. Subfigures in the right hand side are the spectrum calculated from time-domain measurements.

Regarding the parameters extracted from the switching waveform spectrum, the results in Table III to VI show that both time and frequency domain methods can deliver equivalent results in terms of the extracted switching waveform parameters.

For measuring the on-state level of the pulse through the frequency domain measurements it might be required to extrapolate the spectrum envelope to find the amplitude level at the first knee frequency. Contrarily, with the time domain measurements, the state levels can be easily extracted using the histogram method [27]. In the experiments, both methods delivered results with less than 1% of difference for the on-state voltage level.

Concerning the pulse width and rise time, both methods are equally suitable if, in the case of the frequency domain method, the number of harmonic components allows for a smooth representation of the spectrum envelope. However, it must be considered that the rise time measured with the frequency domain method is different, by definition, from the rise-time measured with the oscilloscope. This is because the oscilloscope automated measurement of the rise time is referred to as the 10%-90% interval. If we assume the model of trapezoidal pulse, the rise time measured with the frequency domain approach is expected to be 20% higher than the rise time (10% - 90%) measured with the oscilloscope. This is shown in Table V. If the above consideration is made, both rise time measurements are in excellent agreement with less than 0.3% of difference between them.

TABLE III
ON STATE LEVEL MEASURED USING THE FREQUENCY- AND TIME-DOMAIN METHODS

f_{sw} (MHz)	Frequency domain	Time domain	Difference
0.1	19.4989 V	19.5082 V	-9.3 mV (-0.05%)
1	19.0546 V	19.1624 V	-107.8 mV (-0.56%)
5	18.8365 V	18.8875 V	-51.0 mV (-0.27%)

TABLE IV
SWITCHING FREQUENCY DEVIATION MEASURED USING THE FREQUENCY- AND TIME-DOMAIN METHODS.

f_{sw} (MHz)	Frequency-domain	Time-domain
0.1	0.005 Hz	0.1874 Hz
1	0.005 Hz	17.376 Hz
5	0.005 Hz	108.814 Hz

TABLE V
RISE TIME MEASURED USING THE FREQUENCY- AND TIME-DOMAIN METHODS

f_{sw} (MHz)	Frequency-domain		Time-domain
	$f_{knee_2} = \frac{1}{\pi t_r}$	Rise time	Rise time (10%-90%)
0.1	45.47 MHz	7.004 ns	5.62 ns
1	156.5 MHz	2.034 ns	1.62 ns
5	80.39 MHz	3.935 ns	3.16 ns

TABLE VI
PULSE WIDTH MEASURED USING THE FREQUENCY- AND TIME-DOMAIN METHODS

f_{sw} (MHz)	Frequency-domain		Time-domain	Difference
	$f_{knee_1} = \frac{1}{\pi \tau}$	Pulse width	Pulse width	
0.1	63.72 kHz	4.9959 µs	4.9955 µs	0.008%
1	641.2 kHz	496.43 ns	496.42 ns	0.002 %
5	3.352 MHz	94.961 ns	94.954 ns	0.007 %

The measurement of the switching frequency is much more stable when performed with the spectrum analyzer than with the oscilloscope. This is because the algorithm for the determination mid-reference level instants used in the oscilloscopes is more susceptible to the influence of the overshoot, noise, and distortion in the waveform than a direct measurement of the frequency distance between adjacent harmonic components.

D. Switching losses: measurements vs. simulations

Circuit simulation using SPICE models is a method widely used for predicting the circuit behavior. It is convenient for analyzing the switching losses phenomena since it allows extracting the drain to source voltage and currents required for computing the instantaneous power losses and, therefore, the switching losses.

In our case, LTspice XVII was used to simulate a buck converter based on the topology of the evaluation board used in the experiments. The manufacturer's SPICE model for the EPC2001C GaN FET was used in the simulations. The recommendations in [15] were considered with respect to the layout parasitic inductance. The switching losses were

calculated based on the simulation results for the measured test cases.

Fig. 12 shows a comparison between the simulated and the measured switching losses for a couple of test cases. Simulated losses are significantly lower than the measured ones. This holds for all test cases, as shown in Table VII. The main reason for such differences is related to the longer rise and fall times of the measured waveforms with respect to the simulated ones.

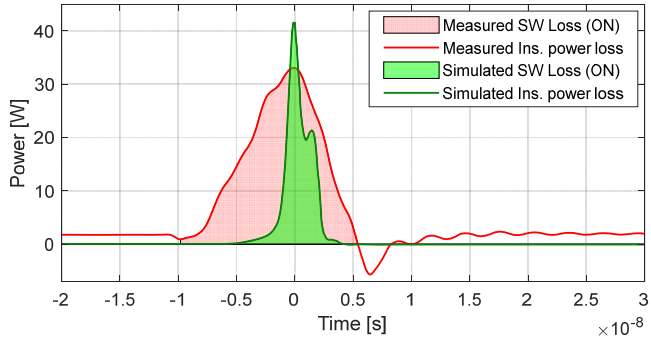

a) f_{sw} = 100 kHz and I_L = 1 A.

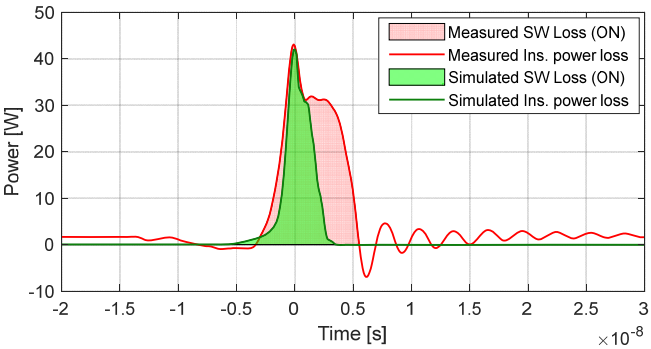

b) f_{sw} = 1 MHz, I_L =1 A

Fig. 12. Measured switching losses versus their predicted value using SPICE simulations.

TABLE VII
SWITCHING LOSSES FOR THE EPC2001C AT THE SPECIFIED OPERATING CONDITIONS

f_{sw} (MHz)	I_L (A)	$E_{on(measurements)}$ (μJ)	$E_{on(simulation)}$ (μJ)
0.1	1	0.249	0,087
1	1	0.203	0,097
5	1	1.700	0,073
0.1	5	0.695	0.460
5	5	0.849	0.331

The difference between the simulated and measured results might be because the model does not consider several factors that are important for a realistic switching losses estimation. For instance, the driver circuit was not simulated in detail, the effect of the rise and fall times of the PWM signal used was not considered or the exact characteristics of the voltage probe and current shunt were not simulated in SPICE.

The simplifications made during the construction of the simulation model seem to have resulted in faster switching transitions and, in consequence, in lower predicted switching losses. Accurate measurements are helpful for determining the representativeness of the simulation models and their reliability for predicting switching losses. A complete analysis of the neglected simulation parameters and their influence in the simulation error is outside the scope of this paper.

VII. MEASUREMENT UNCERTAINTY

A. Analysis of the measurement uncertainty

The analysis of the measurement uncertainty in the switching loss measurement is based on the analytic description of the measurement model using a top-down approach. Then, the sources of uncertainty are propagated and combined flowing the recommendations in the GUM.

Accordingly, the measurement uncertainty in the E_{SW}, u_{SW}, is the combination of the measurement uncertainties of the switching losses during the on and off transitions, u_{ON} and u_{OFF}, respectively. In other words,

$$u_{SW} = \sqrt{(u_{ON})^2 + (u_{OFF})^2}\,. \tag{25}$$

The energy losses in (10) are calculated by integrating the instantaneous power loss during the switching time intervals. In this regard, the measured power loss is a time-discrete vector calculated as the product of the sampled voltage and current waveforms. This means, the energy loss in the time interval $[t_1;\ t_2]$, $E_{[t_1;\,t_2]}$, is estimated by approximating the power integral as a Riemann sum, that is,

$$E_{[t_1;\,t_2]} \approx T_s \sum_{n=n_1}^{n_2} p[nT_s] \tag{26}$$

where T_s is the sampling interval of the waveforms and $n = n_1, n_1 + 1, \ldots, n_2$ is the number of the n-th sample.

Considering the relative timing error in the transition of the switching events, Δ,

$$\Delta = \frac{\sqrt{t_s^2 + t_p^2}}{t_e} \tag{27}$$

where, t_s, t_p and, t_e are the oscilloscope, probe, and edges times, respectively, affects the actual edge time (either rise/fall times), then the integration interval $[t_1;\ t_2]$ is also uncertain. Consequently, the error in the energy loss due to an uncertain time interval, E_Δ, can be bounded as,

$$E_{[t_1+\Delta t_e;\,t_2-\Delta t_e]} \le E_\Delta \le E_{[t_1-\Delta t_e;\,t_2+\Delta t_e]}\,. \tag{28}$$

With no further knowledge about the distribution of E_Δ, a rectangular distribution is assumed and the uncertainty contribution of E_Δ, u_{E_Δ}, is given as

$$u_{E_\Delta} = \frac{E_{[t_1-\Delta t_e;\,t_2+\Delta t_e]} - E_{[t_1+\Delta t_e;\,t_2-\Delta t_e]}}{\sqrt{3}}\,. \tag{29}$$

Assuming independence for the variables in (29), and using the first-order uncertainty propagation rule, the uncertainty in $E_{[t_1;\,t_2]}$, $u_{E_{[t_1;\,t_2]}}$, can be expressed as,

$$u_{E_{[t_1;\,t_2]}} = \sqrt{\left(\frac{E_{[t_1;\,t_2]}}{T_s} u_{T_s}\right)^2 + {T_s}^2 \sum_{n=n_1}^{n_2} {u_{p,n}}^2 + {u_{E_\Delta}}^2} \tag{30}$$

where u_{T_s} is the uncertainty of the sampling interval and $u_{p,n}$ is the uncertainty in the measurement of the instantaneous power loss of the n-th sample. Consequently, $u_{ON} = u_{E_{[t^-_{on};\,t^+_{on}]}}$ and, $u_{OFF} = u_{E_{[t^-_{off};\,t^+_{off}]}}$.

This article has been accepted for publication in a future issue of this journal, but has not been fully edited. Content may change prior to final publication. Citation information: DOI 10.1109/TPEL.2021.3112909, IEEE Transactions on Power Electronics

In this regard, the absolute error of the sampling interval, e_{T_s}, is usually expressed as

$$e_{T_s} = \pm K\, T_s \tag{31}$$

where K is a fixed constant value that represents the combined relative error caused by the elements of the oscilloscope acquisition system, namely, vertical noise, non-linearity, digitizing errors, interleaving errors, aperture uncertainty (sample time jitter), interpolation uncertainty and round-off errors. Therefore, assuming a uniform distribution for e_{T_s}, the standard uncertainty in the sampling interval is,

$$u_{T_s} = \frac{2e_{T_s}}{\sqrt{3}}. \tag{32}$$

Moreover, the $u_{p,n}$ corresponds to the combination of the uncertainty contributions in the voltage, u_v, and current, u_i, waveform points, that is,

$$u_{p,n} = \sqrt{(i_n u_v)^2 + \left(v_n u_{i,n}\right)^2}. \tag{33}$$

where i_n and v_n are the instantaneous value of the current and voltage at the n-th waveform point. With respect u_v, it is quantified as the combination of the sources of uncertainty that limit the accuracy of the oscilloscope vertical system, and it can be expressed as,

$$u_v = \sqrt{(u_{ADC})^2 + (u_{noise})^2 + \left(u_{off}\right)^2 + \left(u_{probe}\right)^2} \tag{34}$$

where u_{ADC}, u_{noise}, u_{off}, and u_{probe} are the uncertainty contributions due to the ADC quantization error, the random noise in the waveforms, the offset error and the combined error due to the oscilloscope probing effects.

On the other hand, the current waveform is measured indirectly through the shunt voltage and using Ohm's law, that is,

$$i(t) = \frac{v_{shunt}(t)}{Z_{shunt}} \tag{35}$$

Therefore, the measurement uncertainty for the n-th current waveform point, $u_{i,n}$, is given by,

$$u_{i,n} = \sqrt{\left[\left(\frac{u_{v_{shunt}}}{Z_{shunt}}\right)^2 + \left(\frac{v_{shunt,n}}{(Z_{shunt})^2} u_{Z_{shunt}}\right)^2\right]} \tag{36}$$

where Z_{shunt} is the nominal value of the shunt impedance, $v_{shunt,n}$ is the n-th shunt voltage waveform point and $u_{Z_{shunt}}$ is the uncertainty in the value of Z_{shunt}. The assigned value and distribution for $u_{Z_{shunt}}$ will depend on the information available on the transducer, i.e. a calibration certificate or a tolerance specification. Finally, the uncertainty in the shunt voltage waveforms points is calculated using the same criterion that in (34).

It is important to highlight that to estimate the uncertainty above, the oscilloscope's specifications must be accounted for in terms of its ADC resolution and the effective number of bits, offset error, gain error, input impedance, etc. In fact, there is no single set of standard figures for defining the accuracy of the oscilloscope vertical system in dynamic conditions. In consequence, from this point onwards, the uncertainty analysis must be made based on the information available for a particular test bench.

As a summary, Figure 13 represents the sources of uncertainty considered in the model above. Finally, the uncertainty in the measurement of the switching losses in terms of power, $u_{P_{SW}}$, can be calculated as,

$$u_{P_{SW}} = \sqrt{(f_{SW} u_{SW})^2 + \left(E_{SW} u_{f_{SW}}\right)^2}, \tag{37}$$

where $u_{f_{SW}}$ is the uncertainty in the measured switching frequency. But, considering that $E_{SW} u_{f_{SW}} \ll f_{SW} u_{SW}$, then the approximation $u_{P_{SW}} \approx f_{SW} u_{SW}$ is sufficiently valid. This means that the measurement uncertainty in the switching power losses are proportional to the switching frequency.

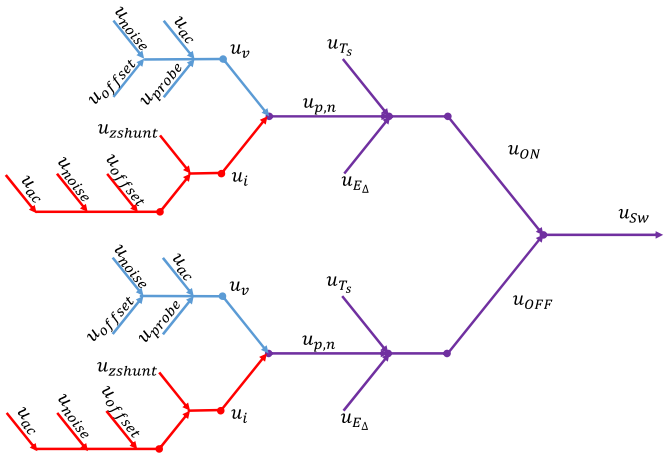

Fig. 13. Contributions to the uncertainty for the switching loss measurement process.

B. Estimation of the measurement uncertainty for the test cases

Based on the specifications of the probe-oscilloscope system formed by the oscilloscope DPO5104B with the passive probes TPP1000 and TDP1500 from Tektronix and the current shunt SDN-414-05 from T&M Research Products, Inc, the measurement uncertainty of the switching losses was calculated using the model above. The results of the evaluation of the measurement uncertainty is presented in Table VIII.

TABLE VIII
MEASUREMENT UNCERTAINTY OF THE SWITCHING LOSSES MEASUREMENT FOR THE TEST CASES EVALUATED.

f_{SW}	I_L	E_{SW}	P_{SW}	$u_{P_{SW}}$		$U_{P_{SW}}$ for $k = 2$	
(MHz)	(A)	(µJ)	(mW)	(mW)	(%)	(mW)	(%)
0.1	1	0.249	24,99	±0.61	±2.42	±1.21	±4.84
1	1	0.203	203.24	±6.22	±3.06	±12.44	±6.12
5	1	1.700	8500.4	±39.9	±0.47	±79.90	±0,94
0.1	5	0.695	69.05	±2.82	±4.08	±5.63	±8.17
5	5	0.849	4245.7	±142.6	±3.36	±285.3	±6.72

Examples of dynamic estimates of the measurement uncertainty propagated to the instantaneous power measurements are shown in Figure 14.

This article has been accepted for publication in a future issue of this journal, but has not been fully edited. Content may change prior to final publication. Citation information: DOI 10.1109/TPEL.2021.3112909, IEEE Transactions on Power Electronics

From the results, it is observed that the measurement uncertainty in the instantaneous power loss increases as the waveforms approaches the instant of maximum losses. This is consistent with the model of the measurement system presented in the previous subsection.

Likewise, it is noticed how the overall uncertainty of the switching loss depends on the actual characteristics and shape of the voltage and current waveforms generated in each transition of the switching device. In the test conditions exercised, the uncertainty in the measurement of the switching loss was between ±1% and ±8%. It is not possible to provide an overall general estimate of the measurement uncertainty resulting from applying this switching loss measurement method, that is, the measurement uncertainty must be calculated for the particular test conditions and test setup.

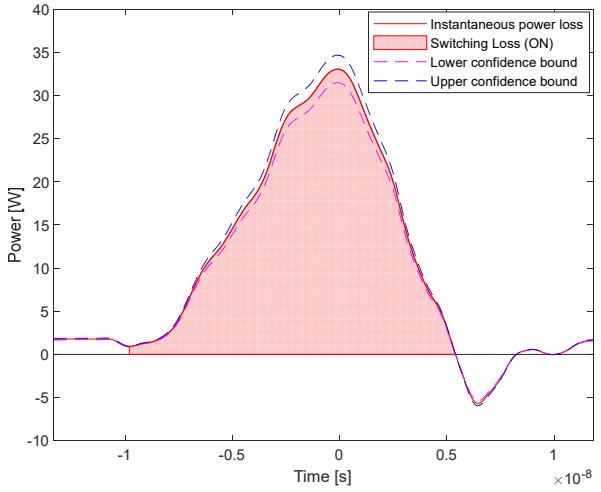

a) f_{sw} =100 kHz, I_L=1 A

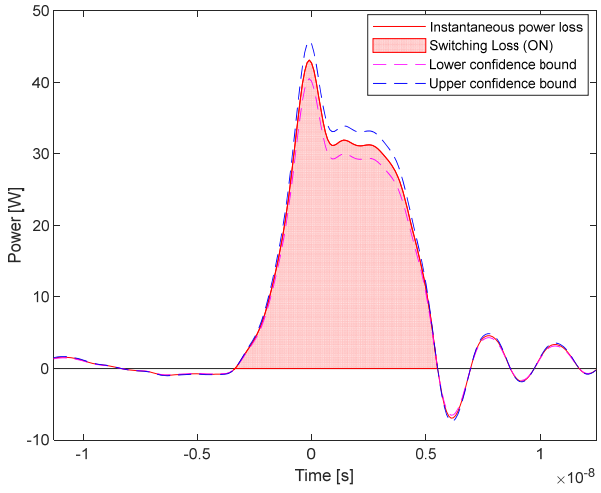

b) f_{sw} =1 MHz, I_L =1 A

Fig. 14. Measurement uncertainty estimates for the instantaneous power losses during the turn-on transition of the EPC2001C GaN FET.

VIII. Conclusion

Using independent methods, the measurement of the switching losses in GaN FETs Power Converters was validated. Excellent agreement (less than 5% of difference) was encountered between the switching losses predicted by the theoretical model and the results from the measurements in the time domain for the different operating conditions exercised. In all cases, the GaN FET was driven within its specified range. This is a reasonable criterion for highly efficient operation of the power converter circuit.

Moreover, the complementary measurements of the spectrum of the switching waveforms were useful for determining if the measured waveforms were subject to distortion because of the band limiting effect of the probe-oscilloscope system. Likewise, using the frequency domain techniques in the characterization of switching losses provides a complementary approach for extracting characteristics of the waveforms such as state level, pulse width, and rise/fall times. This is relevant for determining whether a time-domain measurement system is indeed suitable for the intended application of measuring high-speed waveforms such as those generated by modern GaN FETs when operating in hard-switching applications.

On the other hand, high overshoots may result in discrepancies between time and frequency domain methods for characterizing the switching loss. However, excessive overshoots are usually avoided in DC-DC power converters for the safe operation of the switching device. Therefore, the divergence between time and frequency domain methods is expected to be minor if the overshoots are controlled.

With respect to the comparison between the measured and the predicted values for the switching losses using a SPICE model of the power converter circuit, we obtained comparable peak values for the instantaneous power loss, but major differences in terms of the switching energy losses. The measured switching losses are significantly higher than the predicted ones. Even if this aspect requires further investigation, such differences might be related to the necessary simplifications made in the simulation model. Therefore, simulations may be helpful for obtaining a rough approximation of the switching losses in GaN FETs power converters, but a definitive characterization of such losses requires accurate measurements.

Through the analysis of the measurement uncertainty, it was estimated that, for the experiments presented, the uncertainty was between ±1% and ±8%, which is an excellent result for a test bench formed by general purpose instruments. All the above metrology considerations allow for high quality switching loss measurements with an enhanced understanding of the switching phenomena and insights into the intrinsic limitations of the measurement systems.

Finally, we would like to remark that even if the methods presented in this paper are meant to be generally applicable for characterizing switching losses, they are more valuable when dynamic loss components are predominant, therefore justifying more sophisticated and complex test setups in comparison with traditional means of estimating switching losses. Moreover, accurate, validated, and independent measurement methods are necessary to research the impact of non-linear and parasitic effects in the GaN FET switching phenomena and its implications for more compact and efficient power supplies.

REFERENCES

[1] T. J. Flack, B. N. Pushpakaran, and S. B. Bayne, "GaN Technology for Power Electronic Applications: A Review," *J. Electron. Mater.*, vol. 45, no. 6, pp. 2673–2682, Jun. 2016.

[2] S. Sandler, "Faster-Switching GaN : Presenting a number of interesting measurement challenges," *IEEE Power Electron. Mag.*, vol. 2, no. 2, pp. 24–31, 2015.

[3] D. Jin and J. A. Del Alamo, "Methodology for the study of dynamic ON-resistance in high-voltage GaN field-effect transistors," *IEEE Trans. Electron Devices*, 2013.

[4] M. Okamoto, G. Toyoda, E. Hiraki, T. Tanaka, T. Hashizume, and T. Kachi, "Loss evaluation of an AC-AC direct converter with a new GaN HEMT SPICE model," in *IEEE Energy Conversion Congress and Exposition: Energy Conversion Innovation for a Clean Energy Future, ECCE 2011, Proceedings*, 2011.

[5] L. Wu and M. Saeedifard, "A Simple Behavioral Electro-Thermal Model of GaN FETs for SPICE Circuit Simulation," *IEEE J. Emerg. Sel. Top. Power Electron.*, 2016.

[6] S. Khandelwal *et al.*, "ASM GaN: Industry Standard Model for GaN RF and Power Devices--Part 1: DC, CV, and RF Model," *IEEE Trans. Electron Devices*, pp. 1–7, 2018.

[7] S. A. Albahrani, D. Mahajan, J. Hodges, Y. S. Chauhan, and S. Khandelwal, "ASM GaN: Industry Standard Model for GaN RF and Power Devices--Part-II: Modeling of Charge Trapping," *IEEE Trans. Electron Devices*, pp. 1–8, 2018.

[8] Tektronix, "Measuring Power Supply Switching Loss with an Oscilloscope," in Tektronix Application Notes, pp. 1-12, Sep. 2019. [Online]. Available: https://www.tek.com/document/application-note/measuring-power-supply-switching-loss-oscilloscope

[9] K. Ammous *et al.*, "Error in estimation of power switching losses based on electrical measurements," in *2000 IEEE 31st Annual Power Electronics Specialists Conference. Conference Proceedings (Cat. No.00CH37018)*, 2000, vol. 1, pp. 286–291 vol.1.

[10] K. Ammous, H. Morel, and A. Ammous, "Analysis of Power Switching Losses Accounting Probe Modeling," *IEEE Trans. Instrum. Meas.*, vol. 59, no. 12, pp. 3218–3226, 2010.

[11] K. Ammous, H. Morel, and A. Ammous, "Inverse Models of Voltage and Current Probes," *IEEE Trans. Instrum. Meas.*, vol. 60, no. 12, pp. 3898–3906, 2011.

[12] M. A. Azpúrua, M. Pous, and F. Silva, "Uncertainty Analysis in the Measurement of Switching Losses in GaN FETs Power Converters," in *2020 IEEE International Instrumentation and Measurement Technology Conference (I2MTC)*, 2020, pp. 1–6.

[13] C. Matei, J. Urbonas, H. Votsi, D. Kendig, and P. H. Aaen, "Dynamic Temperature Measurements of a GaN DC–DC Boost Converter at MHz Frequencies," *IEEE Trans. Power Electron.*, vol. 35, no. 8, pp. 8303–8310, 2020.

[14] F. Ziadé, "Final Publishable Report Metrology for advanced energy-saving technology in next-generation electronics applications (16ENG06), Call 2016," 2020. [Online]. Available: https://bit.ly/391quLt

[15] A. Lidow, J. Strydom, M. de Rooij, and D. Reusch, *GaN Transistors for Efficient Power Conversion: Third Edition*. John Wiley & Sons, Ltd, 2019.

[16] K. Wang, M. Tian, H. Li, F. Zhang, X. Yang, and L. Wang, "An improved switching loss model for a 650V enhancement-mode GaN transistor," in *2016 IEEE 2nd Annual Southern Power Electronics Conference, SPEC 2016*, 2016.

[17] M. Crescentini, M. Marchesi, A. Romani, M. Tartagni and P. A. Traverso, "A Broadband, On-Chip Sensor Based on Hall Effect for Current Measurements in Smart Power Circuits," in IEEE Transactions on Instrumentation and Measurement, vol. 67, no. 6, pp. 1470-1485, June 2018, doi: 10.1109/TIM.2018.2795248.

[18] S. J. Nibir, M. Biglarbegian and B. Parkhideh, "A Non-Invasive DC-10-MHz Wideband Current Sensor for Ultra-Fast Current Sensing in High-Frequency Power Electronic Converters," in *IEEE Transactions on Power Electronics*, vol. 34, no. 9, pp. 9095-9104, Sept. 2019, doi: 10.1109/TPEL.2018.2883639.

[19] S. Biswas, D. Reusch, M. de Rooij, and T. Neville, "Evaluation of measurement techniques for high-speed GaN transistors," in *2017 IEEE 5th Workshop on Wide Bandgap Power Devices and Applications (WiPDA)*, 2017, pp. 105–110.

[20] C. Xiao, G. Chen, and W. G. H. Odendaal, "Overview of Power Loss Measurement Techniques in Power Electronics Systems," *IEEE Trans. Ind. Appl.*, vol. 43, no. 3, pp. 657–664, May 2007.

[21] C. R. Paul, *Introduction to Electromagnetic Compatibility: Second Edition*. 2006.

[22] Tektronix, "TPP1000. 1 GHz 10X Passive Probe. Instructions." [Online]. Available: https://download.tek.com/manual/TPP1000-Instructions-071280904.pdf

[23] Tektronix, "MSO5000/DPO5000 Series Mixed Signal Oscilloscopes - Datasheet," 2018. [Online]. Available: https://download.tek.com/datasheet/MSO5000-DPO5000-Mixed-Signal-Oscilloscope-Datasheet-9.pdf.

[24] J. A. Ferreira, W. A. Cronje, and W. A. Relihan, "Integration of high frequency current shunts in power electronic circuits," *IEEE Trans. Power Electron.*, vol. 10, no. 1, pp. 32–37, 1995.

[25] B. Lago and R. Eatock, "Coaxial shunt," *Proc. Inst. Electr. Eng.*, vol. 114, no. 9, pp. 1317–1324, 1967.

[26] F. Krug and P. Russer, "Signal processing methods for time domain EMI measurements," *2003 IEEE Int. Symp. Electromagn. Compat. 2003. EMC '03.*, vol. 2, 2003.

[27] "IEEE Standard for Transitions, Pulses, and Related Waveforms," *IEEE Std 181-2011 (Revision of IEEE Std 181-2003)*. pp. 1–71, 2011.

[28] Efficient Power Conversion Corporation, "EPC2001C – Enhancement Mode Power Transistor," in eGaN® FET Datasheet, pp. 1-6, Jun. 2020. [Online]. Available: https://epc-co.com

Marco A. Azpúrua (Senior Member, IEEE) received the B.Sc. in 2008, M.Sc. in 2013 in telecommunications and electrical engineering, respectively, at Universidad Central de Venezuela, Caracas, and Ph.D in electronics engineering from the Universitat Politècnica de Catalunya, Barcelona, Spain, in 2018. He is currently a Researcher with the Electromagnetic Compatibility Group (GCEM) of the UPC, PT Associate Professor at ETSETB-UPC and the Co-Founder and QA Manager at EMC Barcelona.

Marc Pous (Member, IEEE) received the M.Sc. degree in telecommunications engineering and the Ph.D. degree in electronics engineering from Universitat Politècnica de Catalunya, Barcelona (UPC), Spain in 2009 and 2015, respectively. He is a Researcher at the Electromagnetic Compatibility Group of the UPC GCEM and co-founder of EMC Barcelona startup being the Business Manager of the company. Dr. Pous is a member of ISC EMC Europe, Vice-chairman of EMC Europe 2019, and the Treasurer of the IEEE EMCS Spanish chapter.

Ferran Silva (Senior Member, IEEE) received the M.Sc. and Ph.D. degrees in telecommunication engineering from the Universitat Politècnica de Catalunya (UPC), Barcelona, Spain, in 1989 and 1997, respectively. He is currently an Associate Professor in electronics with the Dept. of Electronic Engineering, UPC. Since 1993, he has been the Head of the Electromagnetic Compatibility Group in the same university (GCEM). He is the author of more than 140 publications about EMC in journals, conferences, and books. Dr. Silva was the Chairman of the EMC Europe International Symposium editions in Barcelona, in 2006 and 2019. Since 2004 he has been Member of the ISC EMC Europe.